ROYAL SOCIETY OF CHEMISTRY

PAPER

Check for updates

Sorption enhanced dimethyl ether synthesis under industrially relevant conditions: experimental validation of pressure swing regeneration

Jasper van Kampen, [iD] *[ab] Jurriaan Boon,[ab] Jaap Vente[a] and Martin van Sint Annaland[b]

Dimethyl ether (DME) is one of the most attractive alternative fuel solutions under consideration worldwide. However, its production from CO_2-rich feedstock or CO_2 directly is limited *via* conventional processes and therefore considered unattractive. For CO_2 utilisation, the production and efficient handling of steam remains a major bottleneck. Sorption enhanced DME synthesis (SEDMES), which combines heterogeneous catalysis with *in situ* water adsorption, is a promising process intensification strategy for the direct production of DME from CO_2. In this work, SEDMES is demonstrated experimentally on a bench-scale reactor with pressure swing regeneration under industrially relevant conditions. Pressure swing regeneration, rather than the time and energy intensive temperature swing regeneration, shows high performance with over 80% single-pass carbon selectivity to DME. This already allows for a factor four increase in productivity, with further optimisation still possible. With the proposed Sips working isotherm for the water adsorbent, and the methanol synthesis and dehydration kinetics, the validated dynamic cycle model adequately describes the SEDMES bench-scale data. Applying shorter cycle times, made possible by pressure swing regeneration, allows optimisation of the DME productivity while maintaining the high single-pass yield typical for SEDMES. The experimental confirmation shown in this paper unlocks the full potential of the high efficiency carbon and hydrogen utilisation by SEDMES technology.

1. Introduction

Dimethyl ether (DME) is the simplest ether compound, with a chemical formula of CH_3OCH_3. DME is gaseous at ambient conditions, which is easy to liquefy and transport. It is safely stored and handled and does not form explosive peroxides in contrast to several other ethers. Its chemical and physical properties as well as its combustion characteristics make that DME can be used as fuel in domestic applications replacing LPG, in compression ignition engines (100% DME) and spark ignition engines (30% DME/70% LPG), and in power generation. Consequently, DME is one of the most promising alternative fuel solutions among the various ultra clean, renewable, and low-carbon fuels under consideration worldwide.[1–3]

Conventionally, DME is produced from synthesis gas with methanol as an intermediate chemical. The following equilibrium reactions are involved:

$$\text{Methanol synthesis} \quad CO_2 + 3H_2 \rightleftharpoons CH_3OH + H_2O \quad (1)$$

$$\text{Methanol synthesis} \quad CO + 2H_2 \rightleftharpoons CH_3OH \quad (2)$$

$$\text{Water–gas shift} \quad CO + H_2O \rightleftharpoons H_2 + CO_2 \quad (3)$$

$$\text{Methanol dehydration} \quad 2CH_3OH \rightleftharpoons CH_3OCH_3 + H_2O \quad (4)$$
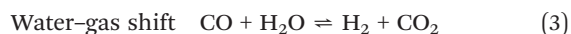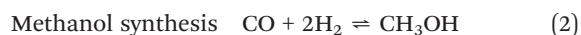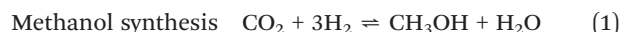
Indirect DME production comprises the production of intermediate methanol (1, 2), and methanol dehydration (4). The incomplete methanol and DME yields require extensive separation sections and recycles. The single-step direct DME synthesis proceeds *via* intermediate methanol as well, yet offers a reduction in process steps and increased overall conversion to DME.[4–7] Although the direct DME synthesis process outperforms the indirect process in terms of efficiency, separation and recycling remain a requirement. In the direct DME synthesis, the O-surplus of the feed ends up in CO_2, resulting in equal molar amounts of DME and CO_2 produced. Since the reaction is equilibrium limited, the downstream separation section produces recycle streams of synthesis gas ($CO + H_2$), CO_2, and methanol. Synthesis gas and methanol can be recycled back to the DME synthesis reactor, while the CO_2 is at best

[a] Sustainable Technologies for Industrial Processes, TNO Energy Transition, P.O. Box 15, 1755 ZG Petten, The Netherlands. E-mail: jasper.vankampen@tno.nl
[b] Chemical Process Intensification, TU/e, P.O. Box 513, 5600 MB Eindhoven, The Netherlands. E-mail: j.v.kampen@tue.nl

244 | *React. Chem. Eng.*, 2021, **6**, 244–257

This journal is © The Royal Society of Chemistry 2021

recycled in synthesis gas generation *via* dry or tri-reforming.[8-15] However, starting from a renewable, CO_2-rich feedstock and/or captured CO_2 to produce DME this is not an option. In fact, one of the major challenges in power-to-liquid (PtL) processes is the direct utilisation of CO_2,[16] making most approaches for renewable fuel production unattractive.[17] For CO_2 utilisation, the production and efficient handling of steam remains a major bottleneck.[18-20]

Separation enhancement is a proven strategy to overcome conversion problems in equilibrium-limited reactions. According to Le Chatelier's principle, the removal of one of the products will shift the equilibrium-limited conversion to the products' side, which is utilised mainly for various CO_2 separation and utilisation processes.[8,21,22] In particular, sorption enhanced DME synthesis (SEDMES) is a novel process route for the production of DME.[23-25] It is based on the *in situ* removal of water by a solid adsorbent, typically a LTA zeolite.[8,26] The *in situ* removal of H_2O assures that the oxygen surplus of the feed no longer ends up as CO_2, as is the case for direct DME synthesis. As a result, CO_2 can be used directly as feed, rather than being the main by-product of DME synthesis.

Sorption enhanced DME synthesis is a promising process intensification strategy for the direct production of DME from CO_2.[7,8,24,26-28] While enabling increased single-pass conversion and selectivity, experimental studies have indicated that time and energy intensive temperature swing regeneration would be required for adsorbent regeneration.[8,26] Pressure swing regeneration is faster and more energy efficient as indicated in a previous SEDMES modelling study[26] and highlighted in our most recent communication.[29]

In this paper the results of an experimental investigation into the bench-scale sorption enhanced production of DME are elaborated, including model validation. The materials involved in SEDMES are tested separately under relevant conditions and combined for sorption enhanced DME production. As in the direct synthesis of DME, a copper–zinc oxide–alumina (CZA) methanol synthesis catalyst is used in combination with methanol dehydration catalyst γ-alumina. In addition, a solid steam adsorbent, LTA zeolite, is required. Proof-of-concept for sorption enhanced DME synthesis is shown with the best (commercially available) materials, model development and validation under industrially relevant conditions (TRL4) are performed. Special attention is being paid to the mode of regeneration, as the key to an economically attractive process.

In the next section, the used materials, the experimental procedures and model interpretation are reported. In the results and discussion section, firstly, the sorbent and catalyst performances are discussed separately for their input in the SEDMES model validation. This is followed by extensive SEDMES testing, model validation and prediction. Finally, the conclusions are summarized.

2. Experimental

Materials

Experimental validation of sorption enhanced DME synthesis was performed using (a homogeneous mixture of) commercially available catalyst and adsorbent: CZA catalyst, γ-Al_2O_3 (assay >98%, Riogen NJ, USA), obtained as 3 mm pellets, and molecular sieve type 3A, purchased as 1.6 mm pellets (UOP Molecular Sieves, Advanced Specialty Gas Equipment, USA).

Methods

The commercially obtained zeolite 3A adsorbent was tested at both atmospheric and high-pressure setups to determine its working capacity at relevant conditions.

Fig. 1 represents the 'Microflow 5' test-rig for atmospheric experiments. A quartz reactor with an internal diameter of 10 mm was filled with 0.1–2 gram of material. During adsorption 100 ml_N min^{-1} was fed to the reactor at 200–300 °C. The gas mixture contained 5–40 mol% H_2O, 5% CH_4 as tracer and balance N_2. Regeneration is performed by switching the gas flow to dry N_2 and, in some cases, increasing the temperature to 350 °C for 5 minutes. Off-gas analysis was performed continuously by a Perkin Elmer Frontier FTIR with heated Pike 2.4 m gas cell. After the experiment, the final mass of the sorbent is determined, and this value is used to calculate the adsorption capacity of each cycle.

Adsorbent and catalyst testing at high pressure were performed similarly, but were conducted on the high-pressure multi-column rig ('Spider', Fig. 1). Samples of initially 0.5 gram catalyst or 5 gram adsorbent were tested. The reactors of 9.2 mm internal diameter are electrically heated and can be run at elevated pressure. During adsorption and/or reaction, the reactors were each fed with 100–150 ml_N min^{-1} of gas mixtures at 200–300 °C and 5–30 bar(a) pressure. The gas mixtures consisted of 10–15 mol% water for adsorbent testing or various syngas ratios for catalyst testing and 5 mol% argon as tracer in balance nitrogen. Adsorbent regeneration always consisted of periodic decreasing the pressure and switching to dry, inert gas. In several settings, the temperature was additionally increased to 250–400 °C. For every setting, the adsorption and the regeneration were measured for every sample. Gas analysis was performed by a gas chromatograph (GC, equipped with a TCD and a FID detector) and a mass spectrometer (MS) measuring hydrogen (m/z = 2), water (m/z = 18), carbon monoxide/nitrogen (m/z = 28), argon (m/z = 40), carbon dioxide (m/z = 44) and DME (m/z = 46).

The experimental procedure for the γ-alumina catalyst testing can be found in previous work.[27]

A combination of commercially obtained CZA catalyst, γ-Al_2O_3 catalyst and zeolite 3A adsorbent were used for the experimental demonstration of direct DME synthesis from $CO/CO_2/H_2$-mixtures.

The experimental runs were conducted on a bench-scale high-pressure reactor setup (Fig. 2), allowing tests up to 2

This journal is © The Royal Society of Chemistry 2021

React. Chem. Eng., 2021, **6**, 244–257 | **245**
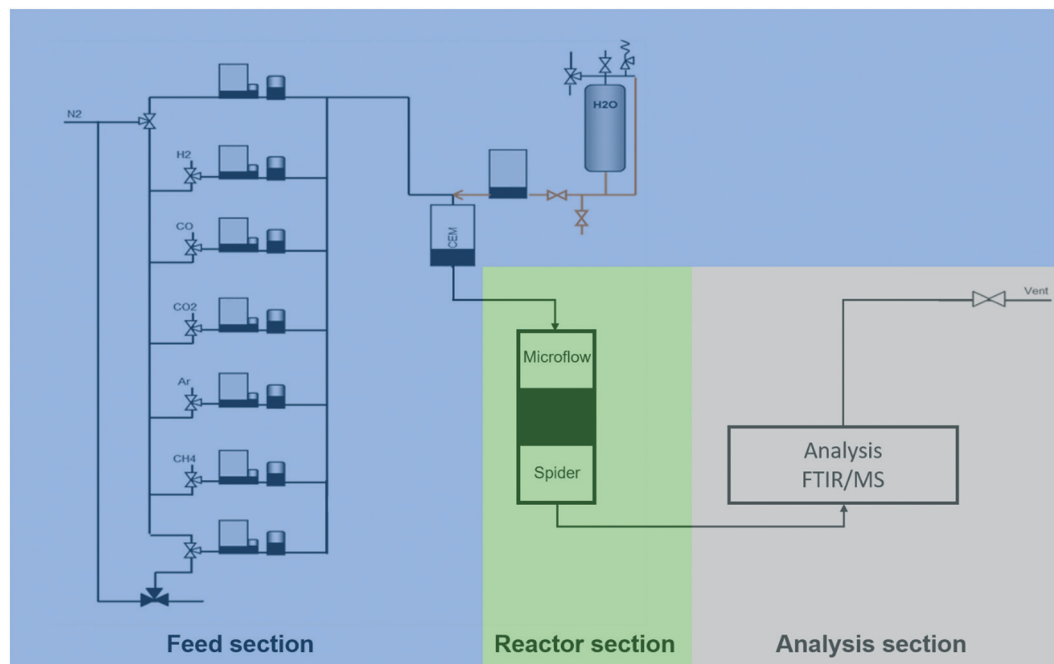
Fig. 1 Schematic presentation of the atmospheric and high pressure reactor units 'Microflow 5' and 'Spider'.

litres of sample, typically consisting of a 1:4 ratio (weight basis) catalyst to sorbent. The ratio between catalyst and sorbent was not further optimised in this work. Adsorption was performed with different (stoichiometric) feed gas compositions, using 68.6–72.7 vol% of hydrogen, 0–9.1 vol% of carbon monoxide, 17.1–23.6 vol% of carbon dioxide and
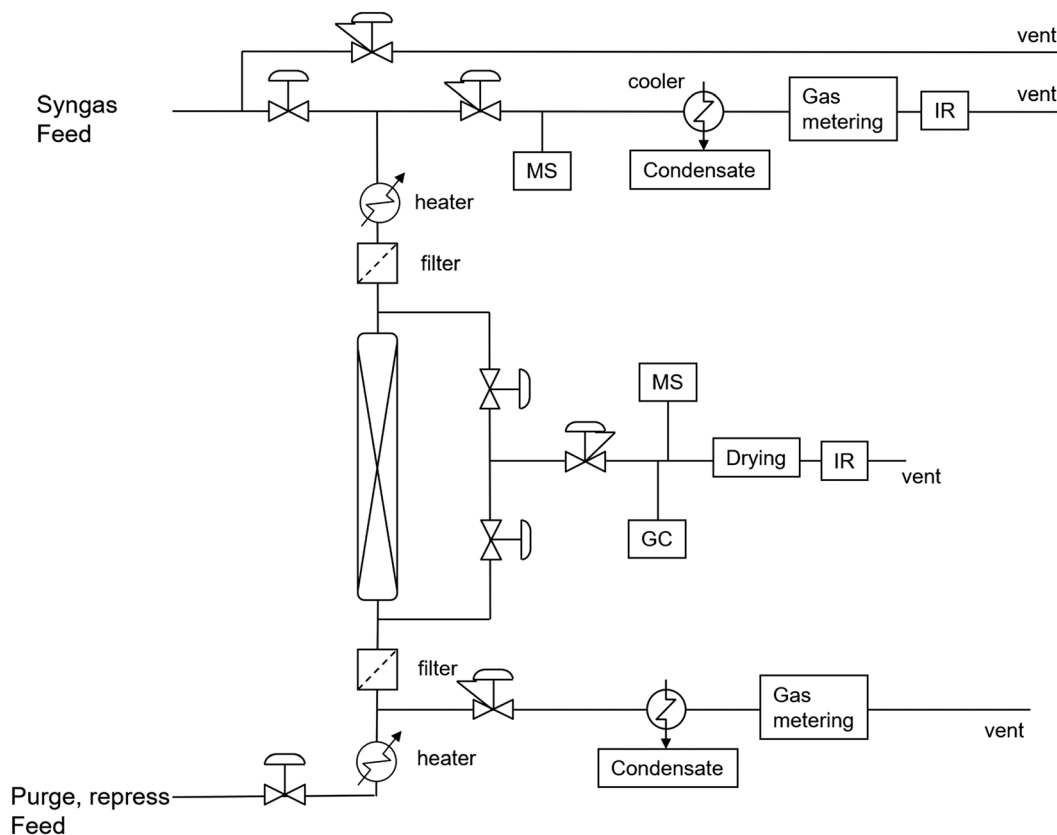

Fig. 2 Schematic of the bench-scale reactor.

246 | *React. Chem. Eng.*, 2021, **6**, 244–257

This journal is © The Royal Society of Chemistry 2021

inert argon, nitrogen or methane, at 25 bar(a) and a temperature range of 250–300 °C. The inert balance was used in order to keep the overall pressure stable, considering the nett mole consumption by the reaction and the adsorption of water. Regeneration was done by depressurisation to 1–3 bar(a) for PSA regeneration, switching to dry, inert gas, and eventual heating to 400 °C for TSA regeneration. Finally, either the inert purge gas or the reactive feed gas is used for repressurisation. Transient gas analysis was performed by micro-GC (measuring methane, CO, CO_2, nitrogen, argon, methanol and DME) and mass spectrometry measuring hydrogen (m/z = 2), methane (m/z = 15), water (m/z = 18), carbon monoxide/nitrogen (m/z = 28), methanol (m/z = 31), carbon dioxide (m/z = 44) and DME (m/z = 45).

Data interpretation

To interpret the breakthrough experiments, a material balance for component i over the reactor column is made. Accumulation of component i between t = 0 and complete breakthrough ($t = t_{end}$) must be equal to the difference between the molar inflow and outflow rates.

$$\frac{y_i(t_{end})pV_g}{RT} + q_i(t_{end})m_{ads} - \frac{y_i(0)pV_g}{RT} - q_i(0)m_{ads}$$
$$= t_{end}F_{i,in} - \int_{t=0}^{t_{end}}(y_i F)_{out}dt \qquad (5)$$

The trapezoidal rule has been used to approximate the integral by a summation over discrete measurement data. The breakthrough of tracer (q_{tracer} = 0), prior to breakthrough of H_2O, is integrated to obtain V_g, the total interparticle and intraparticle gas volume. After breakthrough, the tracer signal is used to quantify the outlet flow rate prior to and during breakthrough and eqn (5) is then used to compute the water loading (q).

In order to facilitate data interpretation, several key metrics have been defined to be able to quantify the SEDMES performance. The most important metric, the carbon selectivity $S(i)$, used here is defined as follows,

$$S(i) = \frac{ny(C_nH_mO_p)}{\sum_i n_i y(i)} \qquad (6)$$

The carbon selectivities were calculated as molar concentration-based selectivities for each of the carbon containing species, $y(i)$. For example, the selectivity towards DME can be calculated as

$$S(DME) = \frac{2y(DME)}{y(CO) + y(CO_2) + 2y(DME) + y(MeOH) + y(CH_4)} \qquad (7)$$

Time integration (in the interval t: $0 - t_{CO_2}$, where t_{CO_2} is the (interpolated) point in time where the CO_2 outlet concentration reaches a level of 5 vol%) of the streams gives an overall yield and selectivity for the cyclic (steady state) performance of the SEDMES process.

Model

A one-dimensional pseudo-homogeneous dynamic reactor model was developed in Matlab, verified and validated.[26] For the description of the fluid flow and mass transfer, the 1D non-steady differential mass and momentum balances are solved. The total mass, momentum, component and overall energy balances are given in Table 1. Reaction kinetics have been determined for the used catalyst materials by fitting the parameters in the models of Graaf *et al.* (1988) and Berčič *et al.* (1992) for the methanol synthesis and methanol dehydration respectively, shown in Table 2.[5,27,30,31] The steam adsorption isotherm of the LTA zeolite adsorbent is determined under the high pressure and temperature working conditions of the SEDMES process. A Sips isotherm best describes the experimental data, in accordance with the available literature at lower temperature and pressure conditions.[32,33] Full details of the different aspects of the model can be found in our previous work.[26]

3. Results and discussion

To investigate the sorption enhanced DME synthesis process further, firstly the adsorption capacity at elevated temperature and pressure is looked into. This is followed by a performance study of the catalyst materials used in SEDMES. Proof-of-concept for sorption enhanced DME synthesis at bench-scale is demonstrated experimentally and

Table 1 Reactor model equations

Overall mass balance	$\frac{\partial \rho}{\partial t} = -\frac{\partial \rho v}{\partial z} - \frac{1-\varepsilon_b}{\varepsilon_b}a_p\sum M_i N_i$	(8)
Momentum balance	$\frac{\partial \rho v}{\partial t} = -\frac{\partial \rho v^2}{\partial z} - \frac{\partial P}{\partial z} - G\frac{\rho\|u\|u}{d_p}$	(9)
Species mass balance	$\frac{\partial \rho \omega_i}{\partial t} = -\frac{\partial \rho v \omega_i}{\partial z} + \frac{\partial}{\partial z}\left(D_z\rho\frac{\partial\omega_i}{\partial z}\right) - \frac{1-\varepsilon_b}{\varepsilon_b}a_p M_i N_i$	(10)
Overall energy balance	$\left(\varepsilon_b\rho Cp + (1-\varepsilon_b)\rho_p Cp_p\right)\frac{\partial T}{\partial t} = -\rho Cpu\frac{\partial T}{\partial z} + \frac{\partial}{\partial z}\left(\lambda\frac{\partial T}{\partial z}\right) + \frac{4U(T_w - T)}{d_r}$	(11)
	$+(1-\varepsilon_b)\rho_p\left(\sum -\Delta H_{r,i}r_i + \sum -\Delta H_{ads,i}\frac{\partial\bar{q}_i}{\partial t}\right)$	
Equation of state	$PM = \rho RT$	(12)

This journal is © The Royal Society of Chemistry 2021

React. Chem. Eng., 2021, **6**, 244–257 | **247**

Table 2 Reaction rate equations

Methanol synthesis from CO (Graaf et al.[30])

$$r_{CH_3OH,1} = \frac{k_1 K_{CO} \left[\varphi_{CO} \varphi_{H_2}^{3/2} - \varphi_{CH_3OH} / \left(\varphi_{H_2}^{1/2} K_{p1} \right) \right]}{\left(1 + K_{CO} \varphi_{CO} + K_{CO_2} \varphi_{CO_2} \right) \left[\varphi_{H_2}^{1/2} + \left(K_{H_2O} / K_{H_2}^{1/2} \right) \varphi_{H_2O} \right]} \tag{13}$$

Water–gas shift (Graaf et al.[30])

$$r_{CO} = \frac{k_2 K_{CO_2} \left[\varphi_{CO_2} \varphi_{H_2} - \varphi_{H_2O} \varphi_{CO} / K_{p2} \right]}{\left(1 + K_{CO} \varphi_{CO} + K_{CO_2} \varphi_{CO_2} \right) \left[\varphi_{H_2}^{1/2} + \left(K_{H_2O} / K_{H_2}^{1/2} \right) \varphi_{H_2O} \right]} \tag{14}$$

Methanol synthesis from CO_2 (Graaf et al.[30])

$$r_{CH_3OH,2} = \frac{k_3 K_{CO_2} \left[\varphi_{CO_2} \varphi_{H_2}^{3/2} - \varphi_{CH_3OH} \varphi_{H_2O} / \left(\varphi_{H_2}^{3/2} K_{p3} \right) \right]}{\left(1 + K_{CO} \varphi_{CO} + K_{CO_2} \varphi_{CO_2} \right) \left[\varphi_{H_2}^{1/2} + \left(K_{H_2O} / K_{H_2}^{1/2} \right) \varphi_{H_2O} \right]} \tag{15}$$

Methanol dehydration (Berčič et al.[31])

$$r_{DME} = \frac{k_4 K_{CH_3OH}^2 \left[C_{CH_3OH}^2 - C_{H_2O} C_{DME} / K_{p4} \right]}{\left[1 + 2 (K_{CH_3OH} C_{CH_3OH})^{1/2} + K_{H_2O} C_{H_2O} \right]^4} \tag{16}$$

the cycle design is discussed as the way forward to enhance productivity and carbon selectivity.

Steam adsorbent

In contrast to typical conditions for water adsorption, sorption enhanced DME synthesis requires good sorbent material performance at elevated temperature and pressure.[8] Based on available open literature, selected adsorbents were tested.[8,32–58] Next to the physically adsorbing zeolite 3A, 4A and 13X samples, three chemical adsorbents were also tested: LHMC, HHMC, and hydrotalcite. Their performance in terms of the cyclic working capacity for steam adsorption was rather disappointing (~1 mol kg^{-1}), therefore they have been disregarded for sorption enhanced DME synthesis.

For the most promising SEDMES adsorbent, LTA zeolite 3A, a working isotherm is determined (Fig. 3). In accordance with the open literature about water adsorption on zeolite 3A at lower temperature and pressure, the data can be described with a Sips isotherm.[32,33] The isotherm parameters are reported in Table 3. As shown in Fig. 3, the Sips isotherm gives an improved prediction of the working capacity, especially at higher steam partial pressure, over the previously used Langmuir–Freundlich isotherm with half the number of parameters.[26,33]

$$q = q_s \frac{(bP)^{1/n}}{1 + (bP)^{1/n}} \tag{17}$$

$$b = b_0 e^{-E_a/RT} \tag{18}$$

Catalyst performance

The copper–zinc oxide–alumina (CZA) methanol synthesis catalyst is tested separately, and in combination with the methanol dehydration catalyst γ-alumina. As shown in Fig. 4, clearly the DME production is far from equilibrium under direct DME synthesis conditions, whereas the methanol production is close to equilibrium for methanol synthesis (greater than equilibrium in DME synthesis) at temperatures over 250 °C. The optimum temperature for methanol synthesis shifts by dilution of the CZA catalyst from 230 to 250 °C, which is well aligned with temperatures reported for methanol and direct DME synthesis in literature.[5,6,26,30,59–67] DME synthesis, however, is far from equilibrium for all catalyst compositions and the DME yield keeps increasing with temperature.[6,68] Despite the fact that the temperature for methanol dehydration is generally higher,[4,27,31,69] direct DME synthesis is often performed at temperatures of around 250 °C,[5,6,26,59–62] not only because the methanol synthesis is considered to be the rate determining step in direct DME
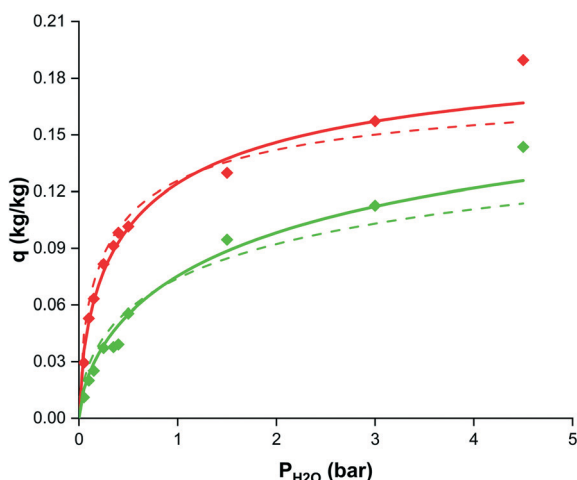

Fig. 3 Working capacity *versus* steam partial pressure based on breakthrough experiments for zeolite 3A at 200 °C (red diamonds) and 250 °C (green diamonds), the isotherm prediction in this work (solid lines) and the isotherm prediction from[33] (dashed lines).

Table 3 Parameters for the Sips isotherm

Parameter	Value
q_s (kg kg^{-1})	0.21
b_0 (bar^{-1})	4.10 10^{-7}
E_a (kJ mol^{-1})	−60.1
n (−)	1.53

248 | *React. Chem. Eng.*, 2021, **6**, 244–257

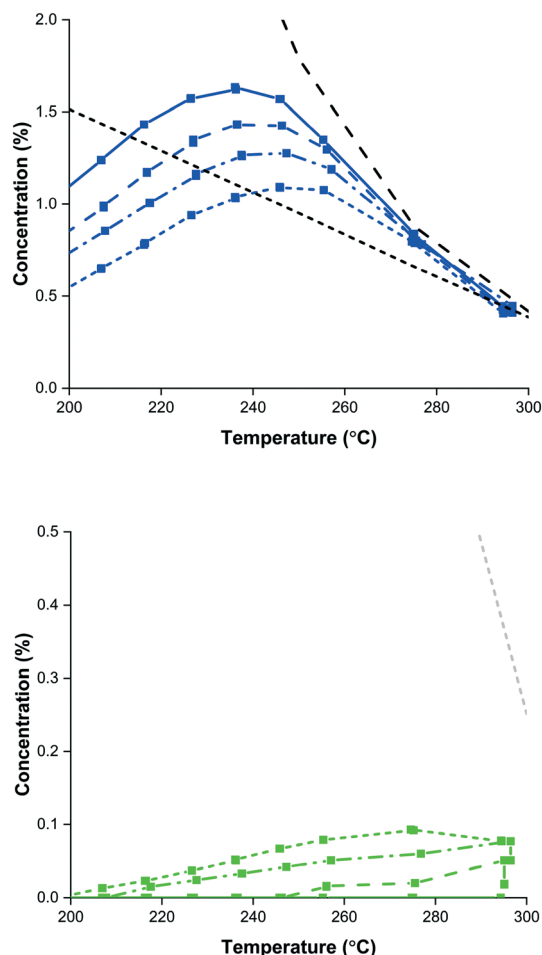This journal is © The Royal Society of Chemistry 2021

Fig. 4 Methanol (top, blue) and DME (bottom, green) concentration in direct synthesis for CO_2 feed at 25 bar and 200–300 °C. The catalyst ratio CZA : alumina is 1 : 0 (solid), 4 : 1 (long dash), 2 : 1 (dash dot) and 1 : 1 (short dash). Methanol equilibrium (black) and DME equilibrium (grey) values in methanol synthesis (dash) and direct DME synthesis (short dash).

synthesis, but also to prevent deactivation of the CZA catalyst at temperatures above 300 °C.

In literature methanol to acidic catalyst ratios of 1 : 1 up to 8 : 1 can be found.[5,6,60,70–74] The rate limiting methanol synthesis is reason to choose higher amounts of methanol synthesis catalyst. However, Fig. 4 shows the limited dehydration in the direct synthesis from CO_2. It is well known that a small amount of CO_2 in the synthesis gas enhances methanol synthesis kinetics,[75] which is not the case with CO_2 as the feed. The additional water present due to CO_2 conversion (eqn (1)), which cannot be converted in the WGS reaction (eqn (3)) due to the absence of CO, limits the dehydration of methanol over γ-alumina.

The performance of γ-alumina is studied under typical methanol dehydration and SEDMES conditions.[27] High activity and selectivity for DME production from methanol at 250 °C are found. However, adsorbed steam reduces the catalytic activity. This deactivation can be caused by the competing adsorption of water, dimers, trimers, or even

larger alcohol–water clusters, but also the (reversible) formation of (surface) boehmite was shown.[27] Despite the large attention for more active low-temperature methanol dehydration catalysts,[4,6,59,69,71,73,74,76–95] γ-Al_2O_3 remains the catalyst of choice for industrial DME production, due to its low cost, high surface area, good thermal and mechanical stability, and high selectivity to DME because its relatively weak Lewis acid sites do not promote side reactions.[4,70,96,97] In contrast to direct DME synthesis, SEDMES offers two specific advantages for the (γ-Al_2O_3) catalyst: the system is operated at low steam pressures and is periodically regenerated due to its adsorptive nature. In fact, the reduced steam content will likely promote deactivation (coking) of other, more acidic, dehydration catalysts.[59,76]

Reaction kinetics for the used materials are determined by fitting the parameters in the methanol synthesis and dehydration reaction models from Graaf et al. (1988) and Berčič et al. (1992) respectively.[26,30,31] The new parameters are given in Table 4 and their good predictive capability of the observed concentrations is shown in Fig. 5. For methanol synthesis the average deviation is less than 5%, which is similar for the DME concentration. Only the methanol concentration in the dehydration experiments shows a higher deviation (11%) due to increased experimental error by feeding liquid methanol at varying conditions.[27] The activation energies determined for the methanol synthesis kinetics are lower than the values originally reported, especially considering the conversion of CO, resulting from a higher activity catalyst.[30] This corresponds with activity factors larger than one reported for present-day methanol synthesis catalysis.[28,67] Also a difference in catalyst activity for methanol dehydration is observed, where the activation energy is changed 24% compared to the original value.[31] The altered value aligns well with modifications of the methanol dehydration kinetics reported for direct DME synthesis in the open literature.[5]

Sorption enhanced DME synthesis

Proof-of-concept for sorption enhanced DME synthesis is demonstrated experimentally at a 2 litre bench-scale reactor (TRL4), already a large step forward in the development of the SEDMES process.[8] Fig. 6 shows a representative

Table 4 Model parameters for methanol synthesis and dehydration reaction kinetics[26]

Parameter	Value (kJ mol^{-1})	Deviation from original
E_a (k_1)	68.1	−38%
E_a (k_2)	107	−13%
E_a (k_3)	54.3	−17%
ΔH (K_{CO})	−15.7	−73%
ΔH (K_{CO_2})	−56.0	−17%
ΔH ($K_{H_2O}/K_{H_2}^{1/2}$)	−107	+2.4%
E_a (k_4)	109	−24%
ΔH (K_{CH_3OH})	−69.6	−1.3%
ΔH (K_{H_2O})	−39.3	−4.4%

This journal is © The Royal Society of Chemistry 2021

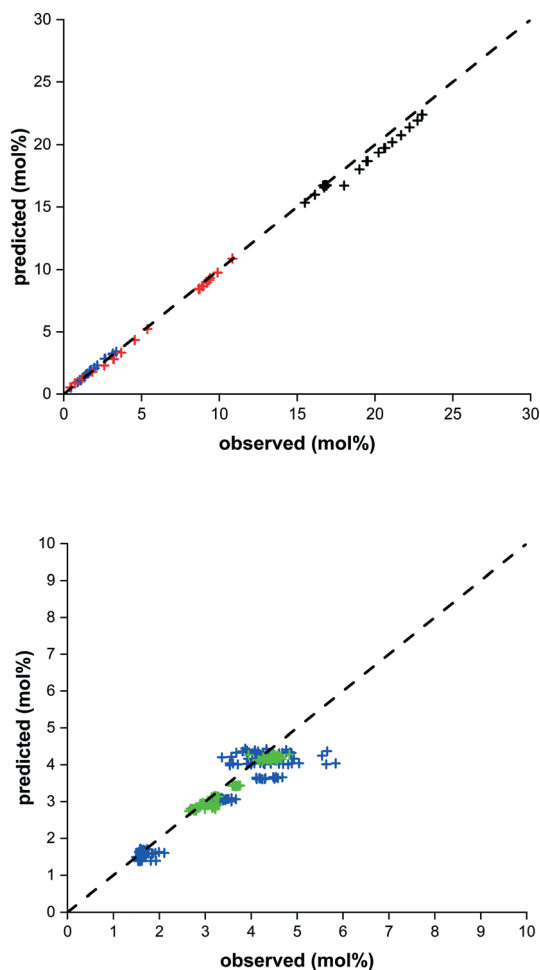React. Chem. Eng., 2021, **6**, 244–257 | **249**

Fig. 5 Parity plot for methanol synthesis (top) and methanol dehydration (bottom). Methanol (blue), DME (green), CO (red) and CO_2 (black).
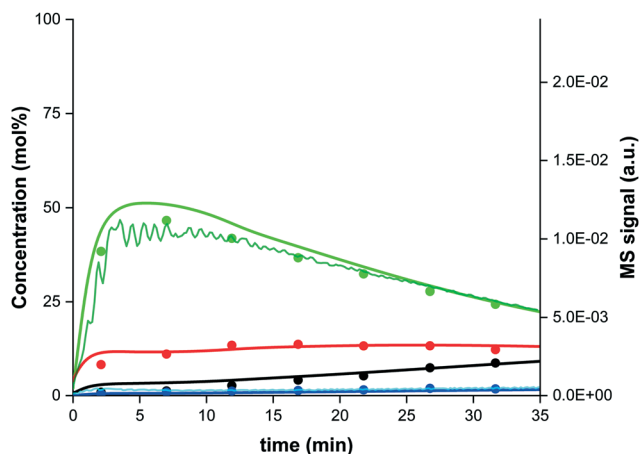

Fig. 6 Experimental data at 250 °C and 25 bar(a) for a $CO_2:CO = 2:1$ feed with stoichiometric hydrogen, without inert, (dots; DME (green), CO (red), CO_2 (black), methanol (blue))[29] and model prediction (lines). MS breakthrough profile of DME (dark green line) and H_2O (light blue line) shown on secondary axis (a.u.).

breakthrough experiment of sorption enhanced DME synthesis. Prior to steam breakthrough, DME and unconverted CO are the primary products. After steam breakthrough the concentration of DME drops, accompanied by the breakthrough of CO_2 and methanol indicating saturation of the adsorbent. As can be seen in Fig. 6 as well, the dynamic cycle model, using the reaction kinetics and water adsorption isotherm as determined in the previous sections, describes the experimental concentration and dynamic behaviour well.

Based on previous modelling work,[26] it was concluded that pressure swing regeneration rather than the so-far required time and energy intensive temperature swing regeneration would be effective. Evaluation of regeneration strategies including pressure swing was therefore among the aims of testing under industrially relevant conditions. The testing under industrially relevant conditions performed in this work indeed proves high performance with pressure swing regeneration, demonstrating over 80% integral carbon selectivity towards DME when using pressure swing regeneration, without the need for a temperature swing (Fig. 6). Where a similar conversion and selectivity can be obtained with pressure swing regeneration (PSA) in comparison with previously reported experiments with a combined temperature and pressure swing regeneration (TPSA), the faster pressure swing regeneration already increases the DME productivity by a factor four, with even further optimisation possible.[29]

One of the optimisation parameters is the carbon selectivity towards DME. Thermodynamically the carbon selectivity to DME is unfavourable and CO_2 will be the main carbon containing product (Fig. 7). However, sorption enhanced DME synthesis allows for a high single-pass carbon conversion to DME irrespective of the carbon source (CO or CO_2), 80% shown here. The model prediction for a $CO_2:CO$ feed of 2:1 is very good (Fig. 7a), and despite a small overprediction for a CO_2 feed (Fig. 7b), the model prediction is still adequate. This overprediction is caused by an apparent catalyst deactivation during the initial part of the experimental campaign, which stabilizes over the full length of the campaign, as shown in Fig. 8. It is well known that especially the CZA catalyst is prone to deactivation under more severe hydrothermal conditions. An advantage of the sorption enhanced reaction conditions include the extremely low water concentration, protecting the catalyst from hydrothermal sintering.[59,70] However, water has also shown to have a positive influence in catalyst deactivation (by coking) for a CO-rich feed. The cause of the observed small decrease in catalyst activity is subject of follow-up work.

Carbon selectivity and productivity

Rather than just a given value, the carbon selectivity can be chosen and optimised by determining the relative time of the reactive adsorption step due to the dynamic nature of sorption enhanced processes. Fig. 9 shows the change in
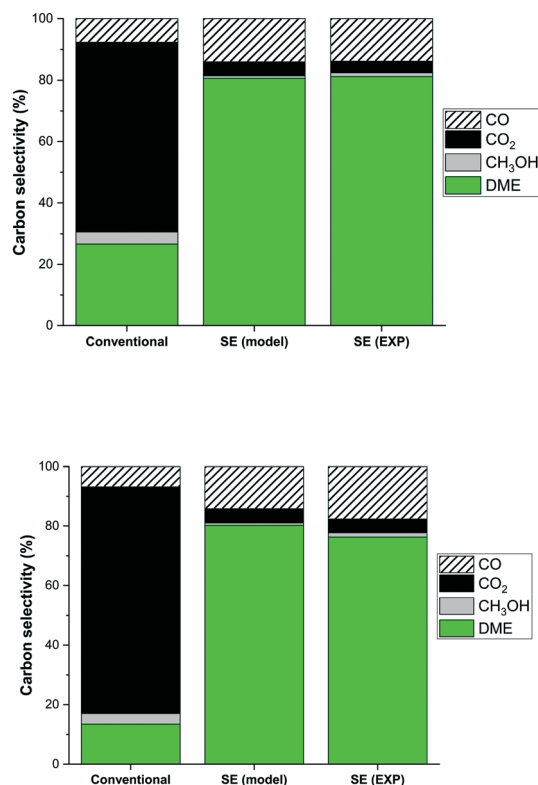
250 | *React. Chem. Eng.*, 2021, **6**, 244–257

This journal is © The Royal Society of Chemistry 2021

Reaction Chemistry & Engineering

Fig. 7 Carbon selectivity for conventional direct DME synthesis (thermodynamic equilibrium), for sorption enhanced DME synthesis model prediction and experimental sorption enhanced DME results at 25 bar(a) and 250 °C for feed: $CO_2 : CO = 2 : 1$ with stoichiometric hydrogen & CH_4 tracer (top) and feed: CO_2 with stoichiometric hydrogen & CH_4 tracer (bottom).

carbon selectivity for the carbon containing species with respect to the adsorption time. Besides optimisation by operating conditions as for conventional processes, the dynamic nature of SEDMES allows extra degrees of freedom and therefore, additional flexibility. Experimental carbon
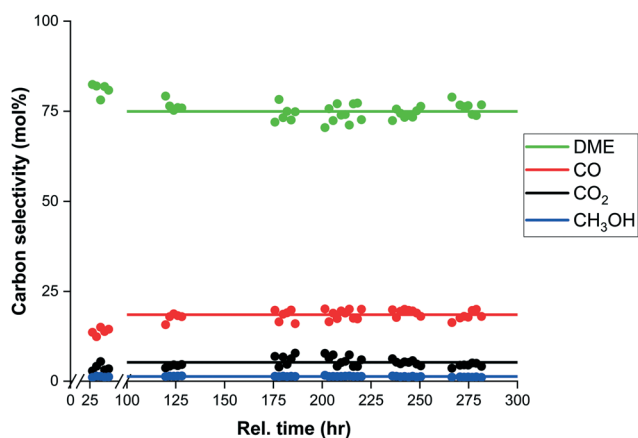

Fig. 8 Apparent catalyst deactivation over relative time (hours), shown by the experimental carbon selectivity (dots) to DME (green), CO (red), CO_2 (black) and methanol (blue).
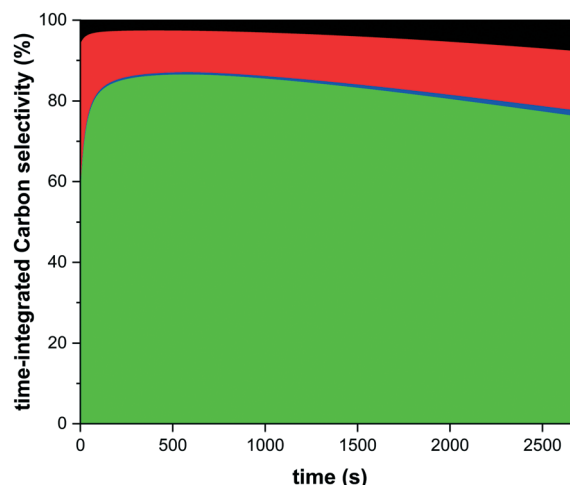

Fig. 9 Integrated cumulative carbon selectivity to DME (green), CO (red), CO_2 (black) and methanol (blue) with respect to the relative time (model prediction for a $CO_2 : CO = 2 : 1$ feed at 25 bar(a) and 250 °C).

selectivity is reported (in other figures) as the integrated selectivity until 5% CO_2 is observed, loosely based on the desired high single-pass conversion of SEDMES and the reduced downstream purification requirements.

The gas hourly space velocity (GHSV) of the feed imposes a trade-off between productivity and selectivity, which is shown in Fig. 10. Regarding this trade-off, the optimal GHSV would be as low as possible from a selectivity point-of-view. Although mass and heat transport eventually would affect the selectivity as well.[26] With increasing GHSV the productivity increases with a loss in selectivity, until the selectivity loss becomes dominant and the productivity will drop as well. In contrast to conventional "steady-state" reaction conditions, the SEDMES process has extra degrees of freedom to optimise the GHSV in combination with the cycle design and timing of the sorption enhanced reaction steps. The selectivity and productivity need to be balanced in the process design and techno-economic evaluation for a specific case.

The duration of the regenerative purge step is one of these additional parameters. A longer purge time results in better regeneration of the system and therefor a higher DME selectivity (Fig. 11), as seen experimentally and well predicted by the model. A longer purge time relative to the adsorption time, however, would require a cycle design with more columns, resulting in a lower overall specific productivity (kg h^{-1} m^{-3}). To decrease the inventory (m^3) and therefore increase the overall productivity a short purge time would be desired. Fig. 11 shows a discrepancy between experimental results and model predictions for a 30 minute purge time. This can be explained by the notion that the experimental data points show a decreasing trend (rather than a spread as is the case for the other data) towards the modelled selectivity.

Fig. 12 shows the experimental results and model predictions accordingly for various combinations of the
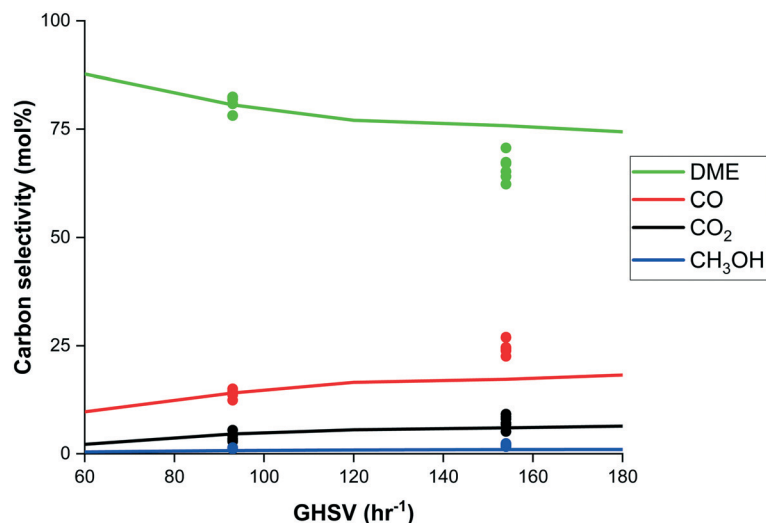
This journal is © The Royal Society of Chemistry 2021

React. Chem. Eng., 2021, **6**, 244–257 | **251**

Fig. 10 Experimental carbon selectivity (dots) to DME (green), CO (red), CO_2 (black) and methanol (blue) and model prediction (lines) as function of feed gas hourly space velocity (h^{-1}).
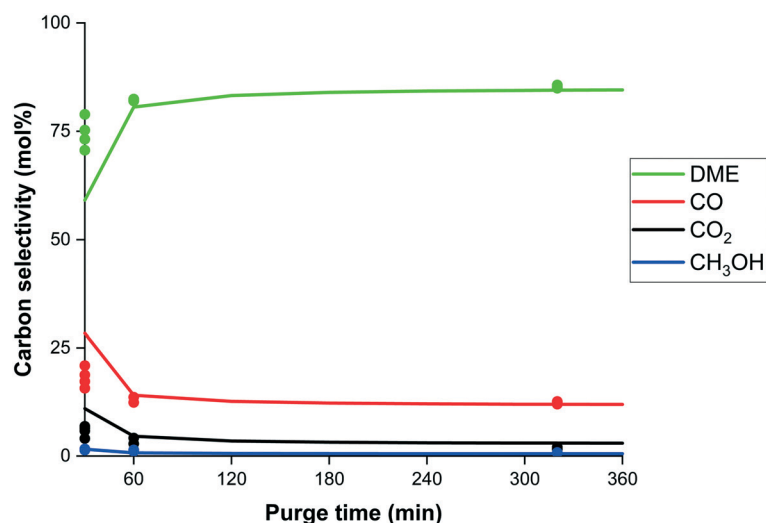

Fig. 11 Experimental carbon selectivity (dots) to DME (green), CO (red), CO_2 (black) and methanol (blue) and model prediction (lines) as function of purge duration (min).

adsorption and regeneration time. It must be noted that the experimental results are based on 2–4 point integration for short timings. Nonetheless, the model predicts the experimental results well for lowering the adsorption and purge time to 20/30 and 10/20 minutes respectively. While the model predicts a significant drop in selectivity for 10/10 minutes due to a decreasing working capacity of the adsorbent, the experimental results show a significantly smaller drop. Investigation of the adsorption behaviour during faster cycling is required to further clarify these observations.

The combination of the adsorption duration (ADS) and regeneration time (DES) allows optimising the trade-off for DME selectivity and productivity, as shown in Fig. 13. Shorter adsorption times potentially result in an increased

production rate. The larger reactor column requirement when the purge time does not decrease with the adsorption time, however, results in a drop in cyclic productivity (kg h^{-1} m^{-3}). Looking at the minimum number of columns required for any given adsorption and purge time, the productivity could be significantly boosted for shorter cycle times with the highest ADS/DES ratio (red bars in Fig. 13). The loss in carbon selectivity predicted by the model for 10/10 minutes would also result in a major drop in predicted productivity (Fig. 12). The promising experimental results, shown in Fig. 13, however indicate that a minor loss in selectivity could still result in increased productivity for faster cycling. The productivities reported in Fig. 13 correspond to 0.04–0.06 kg h^{-1} kg_{cat}^{-1}. This is a major improvement to the previously reported TPSA cycle and close to direct DME pilot plant

252 | *React. Chem. Eng.*, 2021, **6**, 244–257

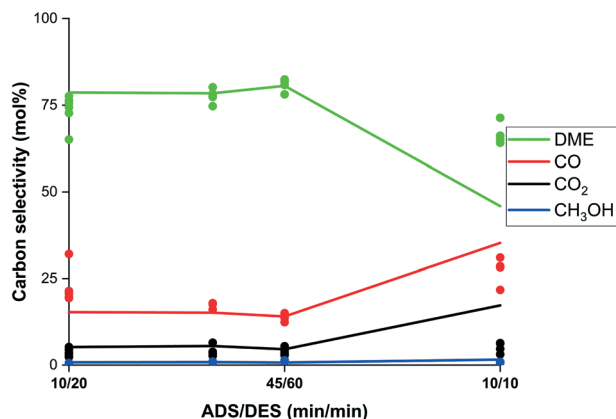This journal is © The Royal Society of Chemistry 2021

Fig. 12 Experimental carbon selectivity (dots) to DME (green), CO (red), CO_2 (black) and methanol (blue) and model prediction (lines) as function of ADS/DES ratio (min min^{-1}).
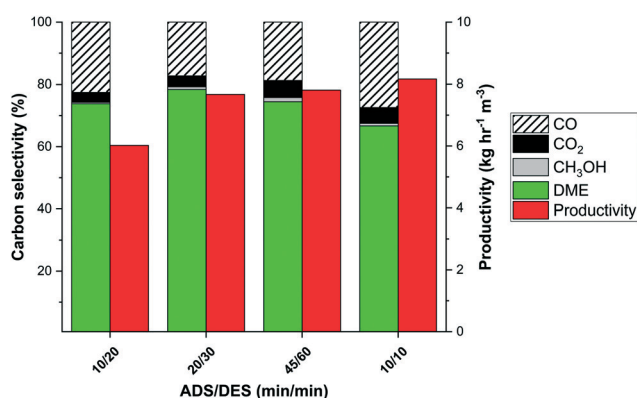

Fig. 13 Experimental carbon selectivity and the productivity for the minimum number of columns (adsorption + purge time; red bars) as function of ADS/DES ratio; integration until 5% CO_2 breakthrough. Conditions: 250 °C and 25 bar(a) for a CO_2:CO = 2:1 feed with stoichiometric hydrogen and CH_4 tracer. Reproduced from ref. 29 with permission from the Royal Society of Chemistry.

productivity for CO to DME, which would strongly deteriorate for CO_2-rich feed.[26]

This increase in productivity shows the impact of the demonstrated PSA regeneration on the SEDMES process performance and thus on the carbon utilisation potential. Benefiting from this work, the cycle design by means of modelling and experimental validation should further unlock the potential of the SEDMES technology as efficient carbon utilisation technology. Followed by techno-economic and life cycles analyses, also the economic and carbon mitigating benefits of SEDMES over conventional DME synthesis technology should be addressed.

4. Conclusions

For the first time, a validated pressure swing regeneration cycle for sorption enhanced DME synthesis (SEDMES) is demonstrated under industrially relevant conditions. SEDMES is a highly flexible process for converting CO_2-rich

(bio-based) syngas and CO_2 directly to DME with a high single-pass conversion, reducing or even eliminating the conventional large recycles and downstream purification sections. The industrially relevant testing performed in this work indeed proves this significant performance, 80% single-pass carbon selectivity to DME demonstrated with pressure swing regeneration, which already allows for a factor four increase in productivity with further optimisation still possible.

The study of the adsorbent material, the catalysts, and the combination of all materials involved resulted in a validated dynamic reactor model, which allows adequate upscaling of the SEDMES technology and predictions of large scale DME synthesis for which faster cycling seems promising to further enhance productivity. Techno-economic and life cycle analyses have to be performed to investigate the economic and carbon mitigating benefits of the high efficiency carbon and hydrogen utilisation by the SEDMES technology.

Nomenclature

a_p	Particle interfacial area (m^2 m^{-3})
b	Isotherm equilibrium constant (bar^{-1})
c_i	Concentration of component i (mol m^{-3})
Cp	Gas thermal conductivity (J kg^{-1} K^{-1})
Cp_p	Particle thermal conductivity (J kg^{-1} K^{-1})
d_p	Particle diameter (m)
D_z	Axial dispersion coefficient (m^2 s^{-1})
E_a	Activation energy (kJ mol^{-1})
G	Ergun constant (−)
ΔH_{ads}	Adsorption enthalpy (J mol^{-1})
$\Delta H_{r,i}$	Reaction enthalpy (J mol^{-1})
k	Reaction rate constant (mol s^{-1} kg^{-1} bar^{-1}) or (kmol kg^{-1} h^{-1})
K_i	Adsorption equilibrium constant of component i (bar^{-1}) or (m^3 kmol^{-3})
K_p	Equilibrium constant (based on partial pressure) (−)
M_i	Molecular weight of component i (kg mol^{-1})
N_i	Mole flux of component i (mol m^{-2} s^{-1})
P	Reactor pressure (bara)
P_i	Partial pressure of component i (bara)
q_i	Adsorbent loading (mol kg^{-1})
q_s	Saturation capacity (kg kg^{-1})
r_i	Reaction rate of component i (mol m^{-3} s^{-1}) or (mol kg^{-1} s^{-1}) or (kmol kg^{-1} h^{-1})
R	Ideal gas constant (J mol^{-1} K^{-1})
t	Time (s)
T	Temperature (K)
u	Superficial gas velocity (m s^{-1})
U	Overall heat transfer coefficient (W m^{-2} K^{-1})
v	Interstitial gas velocity (m s^{-1})
z	Axial coordinate (m)

Greek letters

ε_b	Bed voidage (−)

λ Axial thermal conductivity ($W\ m^{-1}\ K^{-1}$)

ρ Density ($kg\ m^{-3}$)

ρ_p Particle density ($kg\ m^{-3}$)

φ_i Partial fugacity of component i (bara)

ω_i Weight fraction of component i (−)

Conflicts of interest

There are no conflicts to declare.

Acknowledgements

References

1 T. A. Semelsberger, R. L. Borup and H. L. Greene, Dimethyl ether (DME) as an alternative fuel, *J. Power Sources*, 2006, **156**, 497–511.

2 C. Arcoumanis, C. Bae, R. Crookes and E. Kinoshita, The potential of di-methyl ether (DME) as an alternative fuel for compression-ignition engines: A review, *Fuel*, 2008, **87**, 1014–1030.

3 G. A. Olah, A. Goeppert and G. K. S. Prakash, Chemical Recycling of Carbon Dioxide to Methanol and Dimethyl Ether, *J. Org. Chem.*, 2009, **74**, 487–498.

4 U. Mondal and G. D. Yadav, Perspective of dimethyl ether as fuel: Part I. Catalysis, *J. CO2 Util.*, 2019, **32**, 299–320.

5 K. L. Ng, D. Chadwick and B. A. Toseland, Kinetics and modelling of dimethyl ether synthesis from synthesis gas, *Chem. Eng. Sci.*, 1999, **54**, 3587–3592.

6 F. Dadgar, R. Myrstad, P. Pfeifer, A. Holmen and H. J. Venvik, Direct dimethyl ether synthesis from synthesis gas: The influence of methanol dehydration on methanol synthesis reaction, *Catal. Today*, 2016, **270**, 76–84.

7 D. Liuzzi, C. Peinado, M. A. Peña, J. van Kampen, J. Boon and S. Rojas, Increasing dimethyl ether production from biomass-derived syngas via sorption enhanced dimethyl ether synthesis, *Sustainable Energy Fuels*, 2020, **4**, 5674–5681.

8 J. van Kampen, J. Boon, F. van Berkel, J. Vente and M. van Sint Annaland, Steam separation enhanced reactions: Review and outlook, *Chem. Eng. J.*, 2019, **374**, 1286–1303.

9 T. B. H. Nguyen and E. Zondervan, Methanol production from captured CO2 using hydrogenation and reforming technologies_ environmental and economic evaluation, *J. CO2 Util.*, 2019, **34**, 1–11.

10 A. Rafiee, K. Rajab Khalilpour, D. Milani and M. Panahi, Trends in CO2 conversion and utilization: A review from process systems perspective, *J. Environ. Chem. Eng.*, 2018, **6**, 5771–5794.

11 M. T. Luu, D. Milani, M. Wake and A. Abbas, Analysis of di-methyl ether production routes : Process performance evaluations at various syngas compositions, *Chem. Eng. Sci.*, 2016, **149**, 143–155.

12 S.-H. Lee, W. Cho, W.-S. Ju, B.-H. Cho, Y.-C. Lee and Y.-S. Baek, Tri-reforming of CH4 using CO2 for production of synthesis gas to dimethyl ether, *Catal. Today*, 2003, **87**, 133–137.

13 W. Cho, T. Song, A. Mitsos, J. T. McKinnon, G. H. Ko, J. E. Tolsma, D. Denholm and T. Park, Optimal design and operation of a natural gas tri-reforming reactor for DME synthesis, *Catal. Today*, 2009, **139**, 261–267.

14 I. H. Kim, S. Kim, W. Cho and E. S. Yoon, Simulation of commercial dimethyl ether production plant, *20th European Symposium on Computer Aided Process Engineering – ESCAPE20*, ed. S. Pierucci and G. B. Ferraris, 2010, pp. 799–804.

15 S.-H. Lee, W. Cho, T. Song and Y.-J. Ra, Scale up study of DME direct synthesis technology, *Proceedings of World gas conference*, 2009.

16 V. Dieterich, A. Buttler, A. Hanel, H. Spliethoff and S. Fendt, Power-to-liquid via synthesis of methanol, DME or Fischer–Tropsch-fuels: a review, *Energy Environ. Sci.*, 2020, **13**, 3207–3252.

17 R. J. Detz, J. N. H. Reek and B. C. C. van der Zwaan, The future of solar fuels: when could they become competitive?, *Energy Environ. Sci.*, 2018, **11**, 1653–1669.

18 G. Centi and S. Perathoner, Opportunities and prospects in the chemical recycling of carbon dioxide to fuels, *Catal. Today*, 2009, **148**, 191–205.

19 Accelerating Breakthrough Innovation in Carbon Capture, Utilization, and Storage, *Report of the Mission Innovation Carbon Capture, Utilization, and Storage Expert's Workshop*, 2017.

20 A. Katelhon, R. Meys, S. Deutz, S. Suh and A. Bardow, Climate change mitigation potential of carbon capture and utilization in the chemical industry, *Proc. Natl. Acad. Sci. U. S. A.*, 2019, **116**, 11187–11194.

21 A. E. Rodrigues, L. M. Madeira, Y.-J. Wu and R. Faria, *Sorption Enhanced Reaction Processes*, World Scientific, 2017.

22 J. C. Abanades, J. Boon, P. Cobden, K. Coenen, D. S. M. Constantino, R. P. V. Faria, J. R. Fernández, F. Gallucci, M. C. Iliuta, A. E. Rodrigues, E. van Dijk and M. van Sint Annaland, *Sorption Enhancement of Chemical Processes*, Academic Press, 1st edn, 2017.

23 J. Boon, F. van Berkel, H. van Dijk and J. Vente, Separation enhanced dimethyl ether synthesis, *5th TMFB International Conference Aachen*, 2017.

24 I. Iliuta, M. C. Iliuta and F. Larachi, Sorption-enhanced dimethyl ether synthesis — Multiscale reactor modeling, *Chem. Eng. Sci.*, 2011, **66**, 2241–2251.

25 J. van Kampen, J. Boon, F. van Berkel, H. van Dijk, J. Vente and M. van Sint Annaland, Regeneration conditions as the key to sorption enhanced dimethyl ether synthesis, *25th International Symposium on Chemical Reaction EngineeringFlorence*, 2018.

26 J. van Kampen, J. Boon, J. Vente and M. van Sint Annaland, Sorption enhanced dimethyl ether synthesis for high efficiency carbon conversion: Modelling and cycle design, *J. CO2 Util.*, 2020, **37**, 295–308.

27 J. Boon, J. van Kampen, R. Hoogendoorn, S. Tanase, F. P. F. van Berkel and M. van Sint Annaland, Reversible deactivation of γ-alumina by steam in the gas-phase dehydration of methanol to dimethyl ether, *Catal. Commun.*, 2019, **119**, 22–27.

28 S. Guffanti, C. G. Visconti, J. van Kampen, J. Boon and G. Groppi, Reactor modelling and design for sorption enhanced dimethyl ether synthesis, *Chem. Eng. J.*, 2021, **404**, 126573–126585.

29 J. van Kampen, S. Booneveld, J. Boon, J. Vente and M. van Sint Annaland, Experimental validation of pressure swing regeneration for faster cycling in sorption enhanced dimethyl ether synthesis, *Chem. Commun.*, 2020, **56**, 13540–13542.

30 H. Graaf, E. J. Stamhuis and A. A. C. M. Beenackers, Kinetics of low-pressure methanol synthesis, *Chem. Eng. Sci.*, 1988, **43**, 3185–3195.

31 G. Berčič and J. Levec, Intrinsic and Global Reaction Rate of Methanol Dehydration Over γ-Al₂O₃ Pellets, *Ind. Eng. Chem. Res.*, 1992, **31**, 1035–1040.

32 K.-M. Kim, H.-T. Oh, S.-J. Lim, K. Ho, Y. Park and C.-H. Lee, Adsorption Equilibria of Water Vapor on Zeolite 3A, Zeolite 13X, and Dealuminated y Zeolite, *J. Chem. Eng. Data*, 2016, **61**, 1547–1554.

33 E. Gabruś, J. Nastaj, P. Tabero and T. Aleksandrzak, Experimental studies on 3A and 4A zeolite molecular sieves regeneration in TSA process: Aliphatic alcohols dewatering-water desorption, *Chem. Eng. J.*, 2015, **259**, 232–242.

34 Y. Yuan, H. Zhang, F. Yang, N. Zhang and X. Cao, Inorganic composite sorbents for water vapor sorption: A research progress, *Renewable Sustainable Energy Rev.*, 2016, **54**, 761–776.

35 H. Li, C. Qiu, S. Ren, Q. Dong, S. Zhang, F. Zhou, X. Liang, J. Wang, S. Li and M. Yu, Na+-gated water-conducting nanochannels for boosting CO2 conversion to liquid fuels, *Science*, 2020, **367**, 667–671.

36 Z. Pan and C. Y. Zhao, Dehydration/hydration of MgO/H₂O chemical thermal storage system, *Energy*, 2015, **82**, 611–618.

37 A. Kohl and R. Nielsen, Gas Dehydration and Purification by Adsorption, *Gas Purification*, Gulf Publishing Company, 1997.

38 B. Dou, C. Wang, Y. Song, H. Chen, B. Jiang, M. Yang and Y. Xu, Solid sorbents for in-situ CO₂ removal during sorption-enhanced steam reforming process: A review, *Renewable Sustainable Energy Rev.*, 2016, **53**, 536–546.

39 A. Ignatchenko, D. G. Nealon, R. Dushane and K. Humphries, Interaction of water with titania and zirconia surfaces, *J. Mol. Catal. A: Chem.*, 2006, **256**, 57–74.

40 W. Zhu, L. Gora, A. W. C. van den Berg, F. Kapteijn, J. C. Jansen and J. A. Moulijn, Water vapour separation from permanent gases by a zeolite-4A membrane, *J. Membr. Sci.*, 2005, **253**, 57–66.

41 S. Khajavi, J. C. Jansen and F. Kapteijn, Application of hydroxy sodalite films as novel water selective membranes, *J. Membr. Sci.*, 2009, **326**, 153–160.

42 J. Terreni, M. Trottmann, T. Franken, A. Heel and A. Borgschulte, Sorption-Enhanced Methanol Synthesis, *Energy Technol.*, 2019, **7**, 1801093.

43 S. Walspurger, G. D. Elzinga, J. W. Dijkstra, M. Saric and W. G. Haije, Sorption enhanced methanation for substitute natural gas production: Experimental results and thermodynamic considerations, *Chem. Eng. J.*, 2014, **242**, 379–386.

44 B. T. Carvill, J. R. Hufton, M. Anand and S. Sircar, Sorption-enhanced reaction process, *AIChE J.*, 1996, **42**, 2765–2772.

45 J. B. Lad and Y. T. Makkawi, Adsorption of dimethyl ether (DME) on zeolite molecular sieves, *Chem. Eng. J.*, 2014, **256**, 335–346.

46 B. A. V. Santos, V. M. T. M. Silva, J. M. Loureiro and E. Rodrigues, Adsorption of H₂O and Dimethyl Carbonate at High Pressure over Zeolite 3A in Fixed Bed Column, *Ind. Eng. Chem. Res.*, 2014, **53**, 2473–2483.

47 B. Mette, H. Kerskes, H. Drück and H. Müller-Steinhagen, Experimental and numerical investigations on the water vapor adsorption isotherms and kinetics of binderless zeolite 13X, *Int. J. Heat Mass Transfer*, 2014, **71**, 555–561.

48 R. Lin, A. Ladshaw, Y. Nan, J. Liu, S. Yiacoumi, C. Tsouris, D. W. DePaoli and L. L. Tavlarides, Isotherms for Water Adsorption on Molecular Sieve 3A: Influence of Cation Composition, *Ind. Eng. Chem. Res.*, 2015, **54**, 10442–10448.

49 M. Llano-Restrepo and M. A. Mosquera, Accurate correlation, thermochemistry, and structural interpretation of equilibrium adsorption isotherms of water vapor in zeolite 3A by means of a generalized statistical thermodynamic adsorption model, *Fluid Phase Equilib.*, 2009, **283**, 73–88.

50 Q. H. Dirar and K. F. Loughlin, Intrinsic adsorption properties of CO2 on 5A and 13X zeolite, *Adsorption*, 2013, **19**, 1149–1163.

51 K. F. Loughlin, Water isotherm models for 4A (NaA) zeolite, *Adsorption*, 2009, **15**, 337–353.

52 J. Boon, P. D. Cobden, H. A. J. van Dijk, C. Hoogland, E. R. van Selow and M. van Sint Annaland, Isotherm model for high-temperature, high-pressure adsorption of and on K-promoted hydrotalcite, *Chem. Eng. J.*, 2014, **248**, 406–414.

53 A. Borgschulte, E. Callini, N. Stadie, Y. Arroyo, M. D. Rossell, R. Erni, H. Geerlings, A. Züttel and D. Ferri, Manipulating the reaction path of the CO₂ hydrogenation reaction in molecular sieves, *Catal. Sci. Technol.*, 2015, **5**, 4613–4621.

54 R. Delmelle, J. Terreni, A. Remhof, A. Heel, J. Proost and A. Borgschulte, Evolution of Water Diffusion in a Sorption-Enhanced Methanation Catalyst, *Catalysts*, 2018, **8**, 341–355.

55 H. Sun, D. Wu, X. Guo, B. Shen and A. Navrotsky, Energetics of sodium–calcium exchanged zeolite A, *Phys. Chem. Chem. Phys.*, 2015, **17**, 11198–11203.

56 M. Ghodhbene, F. Bougie, P. Fongarland and M. C. Iliuta, Hydrophilic zeolite sorbents for in-situ water removal in high temperature processes, *Can. J. Chem. Eng.*, 2017, **95**, 1842–1849.

57 D. M. Ruthven, *Principles of Adsorption and Adsorption Processes*, Wiley, 1984.

58 R. Plessius, R. Kromhout, L. Dantas, M. Ferbinteanu, M. C. Mittelmeijer-hazeleger, R. Krishna, G. Rothenberg and S. Tanase, Highly Selective Water Adsorption in a Lanthanum Metal – Organic Framework, *Chem. – Eur. J.*, 2014, **20**, 7922–7925.

This journal is © The Royal Society of Chemistry 2021

React. Chem. Eng., 2021, **6**, 244–257 | **255**

59 F. Dadgar, R. Myrstad, P. Pfeifer, A. Holmen and H. J. Venvik, Catalyst Deactivation During One-Step Dimethyl Ether Synthesis from Synthesis Gas, *Catal. Lett.*, 2017, **147**, 865–879.

60 A. García-Trenco and A. Martínez, The influence of zeolite surface-aluminum species on the deactivation of CuZnAl/ zeolite hybrid catalysts for the direct DME synthesis, *Catal. Today*, 2014, **227**, 144–153.

61 S. P. Naik, T. Ryu, V. Bui, J. D. Miller, N. B. Drinnan and W. Zmierczak, Synthesis of DME from CO_2/H_2 gas mixture, *Chem. Eng. J.*, 2011, **167**, 362–368.

62 V. M. Lebarbier, R. A. Dagle, L. Kovarik, J. A. Lizarazo-Adarme, D. L. King and D. R. Palo, Synthesis of methanol and dimethyl ether from syngas over Pd/ZnO/Al2O3 catalysts, *Catal. Sci. Technol.*, 2012, **2**, 2116–2127.

63 S. Dang, H. Yang, P. Gao, H. Wang, X. Li, W. Wei and Y. Sun, A review of research progress on heterogeneous catalysts for methanol synthesis from carbon dioxide hydrogenation, *Catal. Today*, 2019, **330**, 61–75.

64 S. Jadhav, P. Vaidya, B. Bhanage and J. Joshi, Chemical Engineering Research and Design Catalytic carbon dioxide hydrogenation to methanol : A review of recent studies, *Chem. Eng. Res. Des.*, 2014, **92**, 2557–2567.

65 H. J. Venvik and J. Yang, Catalysis in microstructured reactors: Short review on small-scale syngas production and further conversion into methanol, DME and Fischer-Tropsch products, *Catal. Today*, 2017, **285**, 135–146.

66 X. Jiang, X. Nie, X. Guo, C. Song and J. G. Chen, Recent Advances in Carbon Dioxide Hydrogenation to Methanol via Heterogeneous Catalysis, *Chem. Rev.*, 2020, **120**(15), 7984–8034.

67 A. Montebelli, C. G. Visconti, G. Groppi, E. Tronconi, C. Ferreira and S. Kohler, Enabling small-scale methanol synthesis reactors through the adoption of highly conductive structured catalysts, *Catal. Today*, 2013, **215**, 176–185.

68 I. A. Kurzina, S. I. Reshetnikov, N. I. Karakchieva and L. N. Kurina, Direct synthesis of dimethyl ether from synthesis gas: Experimental study and mathematical modeling, *Chem. Eng. J.*, 2017, **329**, 135–141.

69 H. Bateni and C. Able, Development of Heterogeneous Catalysts for Dehydration of Methanol to Dimethyl Ether: A Review, *Katal. Prom-sti.*, 2019, **11**, 7–33.

70 M. Stiefel, R. Ahmad, U. Arnold and M. Döring, Direct synthesis of dimethyl ether from carbon-monoxide-rich synthesis gas : In fl uence of dehydration catalysts and operating conditions, *Fuel Process. Technol.*, 2011, **92**, 1466–1474.

71 A. García-Trenco, S. Valencia and A. Martínez, The impact of zeolite pore structure on the catalytic behavior of CuZnAl/ zeolite hybrid catalysts for the direct DME synthesis, *Appl. Catal., A*, 2013, **468**, 102–111.

72 A. T. Aguayo, J. Erena, D. Mier, J. M. Arandes, M. Olazar and J. Bilbao, Kinetic Modeling of Dimethyl Ether Synthesis in a Single Step on a CuO−ZnO−Al2O3/γ-Al2O3 Catalyst, *Ind. Eng. Chem. Res.*, 2007, **46**, 5522–5530.

73 G. Bonura, M. Cordaro, C. Cannilla, A. Mezzapica, L. Spadaro, F. Arena and F. Frusteri, Catalytic behaviour of a bifunctional system for the one step synthesis of DME by CO_2 hydrogenation, *Catal. Today*, 2014, **228**, 51–57.

74 F. Frusteri, M. Migliori, C. Cannilla, L. Frusteri, E. Catizzone, A. Aloise, G. Giordano and G. Bonura, Direct CO_2-to-DME hydrogenation reaction: New evidences of a superior behaviour of FER-based hybrid systems to obtain high DME yield, *J. CO2 Util.*, 2017, **18**, 353–361.

75 K. Klier, V. Chatikavanij, R. G. Herman and G. W. Simmons, Catalytic synthesis of methanol from CO/H_2, *J. Catal.*, 1982, **74**, 343–360.

76 E. Catizzone, M. Migliori, A. Purita and G. Giordano, Ferrierite vs. γ-Al2O3: The superiority of zeolites in terms of water-resistance in vapour-phase dehydration of methanol to dimethyl ether, *J. Energy Chem.*, 2019, **30**, 162–169.

77 E. Catizzone, S. V. Daele, M. Bianco, A. Di Michele, A. Aloise, M. Migliori, V. Valtchev and G. Giordano, Catalytic application of ferrierite nanocrystals in vapour-phase dehydration of methanol to dimethyl ether, *Appl. Catal., B*, 2019, **243**, 273–282.

78 E. Catizzone, A. Aloise, M. Migliori and G. Giordano, From 1-D to 3-D zeolite structures: performance assessment in catalysis of vapour-phase methanol dehydration to DME, *Microporous Mesoporous Mater.*, 2017, **243**, 102–111.

79 E. Catizzone, A. Aloise, M. Migliori and G. Giordano, Dimethyl ether synthesis via methanol dehydration: Effect of zeolite structure, *Appl. Catal., A*, 2015, **502**, 215–220.

80 V. Barbarossa, R. Viscardi, G. Maestri, R. Maggi, D. Mirabile Gattia and E. Paris, Sulfonated catalysts for methanol dehydration to dimethyl ether (DME), *Mater. Res. Bull.*, 2019, **113**, 64–69.

81 G. Baracchini, A. G. F. Machoke, M. Klumpp, R. Wen, P. Arnold, W. Schwieger and R. Dittmeyer, Structured catalysts for the direct synthesis of dimethyl ether from synthesis gas: A comparison of core@shell versus hybrid catalyst configuration, *Catal. Today*, 2020, **342**, 46–58.

82 S. Baier, C. D. Damsgaard, M. Klumpp, J. Reinhardt, T. Sheppard, Z. Balogh, T. Kasama, F. Benzi, J. B. Wagner, W. Schwieger, C. G. Schroer and J. D. Grunwaldt, Stability of a Bifunctional Cu-Based Core@Zeolite Shell Catalyst for Dimethyl Ether Synthesis Under Redox Conditions Studied by Environmental Transmission Electron Microscopy and In Situ X-Ray Ptychography, *Microsc. Microanal.*, 2017, **23**, 501–512.

83 S. Ren, W. R. Shoemaker, X. Wang, Z. Shang, N. Klinghoffer, S. Li, M. Yu, X. He, T. A. White and X. Liang, Highly active and selective Cu-ZnO based catalyst for methanol and dimethyl ether synthesis via CO2 hydrogenation, *Fuel*, 2019, **239**, 1125–1133.

84 T. A. Semelsberger, K. C. Ott, R. L. Borup and H. L. Greene, Role of acidity on the hydrolysis of dimethyl ether (DME) to methanol, *Appl. Catal., B*, 2005, **61**, 281–287.

85 M. Cai, A. Palčić, V. Subramanian, S. Moldovan, O. Ersen, V. Valtchev, V. V. Ordomsky and A. Y. Khodakov, Direct dimethyl ether synthesis from syngas on copper-zeolite hybrid catalysts with a wide range of zeolite particle sizes, *J. Catal.*, 2016, **338**, 227–238.

256 | *React. Chem. Eng.*, 2021, **6**, 244–257

This journal is © The Royal Society of Chemistry 2021

86 A. Ateka, I. Sierra, J. Ereña, J. Bilbao and A. T. Aguayo, Performance of CuO–ZnO–ZrO2and CuO–ZnO–MnO as metallic functions and SAPO-18 as acid function of the catalyst for the synthesis of DME co-feeding CO2, *Fuel Process. Technol.*, 2016, **152**, 34–45.

87 A. Ateka, P. Pérez-Uriarte, I. Sierra, J. Ereña, J. Bilbao and A. T. Aguayo, Regenerability of the CuO–ZnO–MnO/SAPO-18 catalyst used in the synthesis of dimethyl ether in a single step, *React. Kinet., Mech. Catal.*, 2016, **119**, 655–670.

88 A. Ateka, M. Sánchez-Contador, J. Ereña, A. T. Aguayo and J. Bilbao, Catalyst configuration for the direct synthesis of dimethyl ether from CO and CO2 hydrogenation on CuO–ZnO–MnO/SAPO-18 catalysts, *React. Kinet., Mech. Catal.*, 2018, **124**, 401–418.

89 Y. Wang, W.-L. Wang, Y.-X. Chen, J.-J. Zheng and R.-F. Li, Synthesis of dimethyl ether from syngas using a hierarchically porous composite zeolite as the methanol dehydration catalyst, *J. Fuel Chem. Technol.*, 2013, **41**, 873–880.

90 A. E. A. A. Said, M. M. Abd El-Wahab and M. A. El-Aal, The catalytic performance of sulfated zirconia in the dehydration of methanol to dimethyl ether, *J. Mol. Catal. A: Chem.*, 2014, **394**, 40–47.

91 M. Rutkowska, D. Macina, N. Mirocha-Kubień, Z. Piwowarska and L. Chmielarz, Hierarchically structured ZSM-5 obtained by desilication as new catalyst for DME synthesis from methanol, *Appl. Catal., B*, 2015, **174–175**, 336–343.

92 M. H. Huang, H. M. Lee, K. C. Liang, C. C. Tzeng and W. H. Chen, An experimental study on single-step dimethyl ether (DME) synthesis from hydrogen and carbon monoxide under various catalysts, *Int. J. Hydrogen Energy*, 2015, **40**, 13583–13593.

93 Y. Hua, X. Guo, D. Mao, G. Lu, G. L. Rempel and F. T. T. Ng, Single-step synthesis of dimethyl ether from biomass-derived syngas over CuO-ZnO-MO x (M = Zr, Al, Cr, Ti)/HZSM-5 hybrid catalyst: Effects of MO x, *Appl. Catal., A*, 2017, **540**, 68–74.

94 R. Dębek, M. F. G. Ribeiro, A. Fernandes and M. Motak, Dehydration of methanol to dimethyl ether over modified vermiculites, *C. R. Chim.*, 2015, **18**, 1211–1222.

95 M. Xu, D. W. Goodman and A. Bhattacharyya, Catalytic dehydration of methanol to dimethyl ether (DME) over Pd/Cab-O-Sil catalysts, *Appl. Catal., A*, 1997, **149**, 303–309.

96 E. Catizzone, G. Bonura, M. Migliori, F. Frusteri and G. Giordano, CO2 Recycling to Dimethyl Ether: State-of-the-Art and Perspectives, *Molecules*, 2018, **23**, 31–59.

97 J. Sun, G. Yang, Y. Yoneyama and N. Tsubaki, Catalysis Chemistry of Dimethyl Ether Synthesis, *ACS Catal.*, 2014, **4**, 3346–3356.

This journal is © The Royal Society of Chemistry 2021

React. Chem. Eng., 2021, **6**, 244–257 | **257**